Wang et al. *NPG Asia Materials* (2022) 14:54
https://doi.org/10.1038/s41427-022-00401-8

NPG Asia Materials

ARTICLE Open Access

# Responsive photonic alginate hydrogel particles for the quantitative detection of alkaline phosphatase

Yuetong Wang[1,2], Dagan Zhang[1], Hui Zhang[1], Luoran Shang[3] and Yuanjin Zhao[1]

**Abstract**

Alkaline phosphatase (ALP) is an important marker for many diseases, yet an efficient and reliable detection method is still lacking. Here, we present a novel photonic alginate hydrogel particle as an ALP sensor based on the competitive combination of an intermediary agent, the pyrophosphate ion (PPi), with a hydrogel crosslinker, which can trigger a phase-transition response from the hydrogel. This response can be converted into dual optical readouts, a fluorescence signal and a structural color signal. Quantitative determination of ALP was established based on this dual-indicator system with high accuracy and reliability. These features suggest potential ideal applications of responsive photonic hydrogel particles to detect ALP and other macromolecules.

## Introduction

Alkaline phosphatase (ALP) is a type of extensively distributed enzyme that exists in living species[1]. It plays a crucial role in the dephosphorylation of nucleic acids, proteins, and other biomolecules, thus serving various roles in cellular regulation and signal transduction[2,3]. In addition, a great deal of evidence has revealed that abnormal ALP activity levels could act as crucial prognostic indicators for various diseases, such as disorders of the liver, endocrine system, and bone tissues[4,5]. Hence, the sensitive and specific detection of ALP could help evaluate certain relevant physiological and pathological states. To date, scientists have established many ALP detection strategies, such as colorimetry[6], chemiluminescence[7,8], electrochemistry[9,10], Raman spectroscopy[11], chromatography[12–14], and fluorescent probes[15,16]. Among them, fluorescence assays, which rely on a fluorochrome probe, is a preferable method due to its high sensitivity and specificity[17–19]. These fluorescence-based detection methods have achieved satisfactory results for a wide range of molecules, but most still require specialized instruments and complicated operations for a signal readout[20–22]. To address these limitations, hydrogel materials could be applied as carriers for fluorochrome probes and serve as molecular sensors[23–25]. Such a hydrogel sensor could convert the target molecule signal to an optical readout through the stimuli-responsive phase transition and thus feature a simple detection process[26,27]. However, conventional bulk hydrogel sensors still face the dilemma of a long reaction time, and the accuracy and reliability of detection tend to be limited to a single signal readout[28,29]. Therefore, a novel platform for the efficient and accurate detection of ALP is highly anticipated.

In this paper, we presented a novel hydrogel-based inverse opal microparticle for ALP detection with the desired features, as shown in Fig. 1. Inverse opal particles refer to one type of particulate material with 3D ordered voids[30–32]. Their spherical shape and highly interconnected pores provide a large specific surface area and abundant molecular binding sites[33,34]. In particular, hydrogel-based inverse opal microparticles can efficiently sense specific molecule stimuli through phase transition[35,36]. In addition, the periodic porous architecture of these inverse opal particles gives rise to a photonic effect with the production of color detectable to the naked eye[37–39]. Thus, inverse

Correspondence: Luoran Shang(luoranshang@fudan.edu.cn) or Yuanjin Zhao(yjzhao@seu.edu.cn)
[1]Department of Rheumatology and Immunology, Nanjing Drum Tower Hospital, School of Biological Science and Medical Engineering, Southeast University, 210096 Nanjing, China
[2]School of Food Science and Pharmaceutical Engineering, Nanjing Normal University, 210046 Nanjing, China
Full list of author information is available at the end of the article

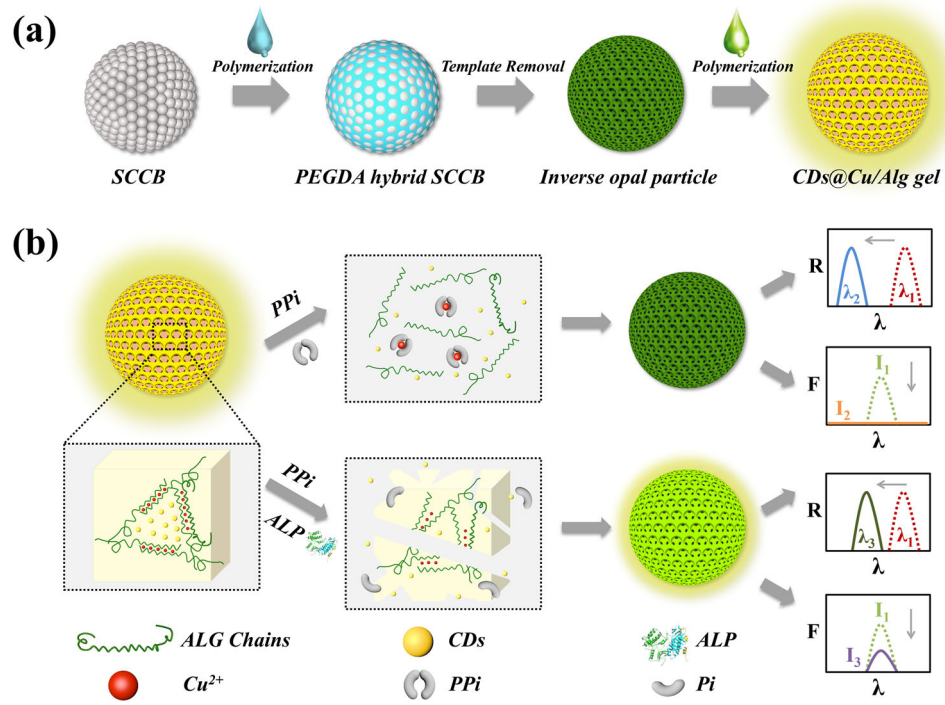


**Fig. 1 Scheme showing the PPi-responsive photonic alginate hydrogel particles for alkaline phosphatase quantitative detection. a** The fabrication process of the hybrid photonic microparticles. **b** The detection mechanism of the hybrid photonic microparticles. When adding PPi, the hydrogel network could be disrupted due to PPi's strong competitive coordination effect with $Cu^{2+}$, resulting in the leakage of inner CDs to the external solution. This could trigger a simultaneous decrease in the fluorescence intensity and blueshift of the reflection spectrum of the particles. ALP can react with PPi and suppress the disintegration of the hydrogel to a certain extent depending on the ALP concentration. Therefore, quantitative detection of ALP could be achieved by measuring the dual optical signals.

hydrogel opal particles have been widely used for the detection of various targets, including ions, small molecules, and biomacromolecules[40,41]. However, most hydrogels do not respond to ALP, making it difficult to detect ALP directly. Thus, a strategy enabling inverse opal hydrogel microparticles to sense the activity of ALP is strongly desired.

Herein, we constructed hybrid microparticles containing a poly(ethylene glycol) diacrylate (PEGDA) inverse opal scaffold embedding an alginate (Alg) hydrogel for ALP detection. The detection mechanism was based on a strong competitive coordination between the intermediary agent, pyrophosphate ion (PPi), and the hydrogel crosslinker $Cu^{2+}$, which resulted in disruption of the hydrogel network. Carbon dots (CDs) were integrated into the hydrogel to produce a fluorescent indicator of the responsive gel-sol transition of the hydrogel. Since ALP can catalyze the hydrolysis of PPi and impede such competitive coordination, ALP could thus be detected quantitatively by measuring the fluorescence intensity of the nanoparticles. In addition, the gel-sol transition leads to a shift in the reflection spectrum of the inverse opal particles, offering another detection approach. Moreover, the PEGDA skeleton possesses favorable mechanical strength and maintains stability and integrity during the detection processes. These features make these hybrid photonic hydrogel particles ideal for the detection of ALP and extend the application value of hydrogel-based optical sensors.

## Materials and methods

### Materials

Alginate, sodium pyrophosphate, copper chloride, and metal salts were purchased from Aladdin, Shanghai, China. ALP was purchased from Sangon Biotech, Shanghai, China. Poly(ethylene glycol) diacrylate (PEGDA 700) was purchased from Sigma–Aldrich. Aqueous dispersions of CDs with a maximum emission wavelength at 535 nm were purchased from Suzhou Xingshuo Nanotech Co.

### Preparation of Alg/Cu gel and CDs@Alg/Cu hydrogel

The copper alginate hydrogel was obtained by simply mixing 200 μL of 1 wt% alginate pregel and 200 μL of 2 mM $CuCl_2$ aqueous solution. Gelation occurred within 1 h at room temperature. After that, the copper alginate hydrogel was washed three times. Then, 200 μL of CDs

were mixed with 200 μL of 2 wt% alginate aqueous solution with shaking for 30 min. Then, we added 400 μL of 2 mM $CuCl_2$ aqueous solution to this system. After reacting for 1 h, the insoluble fluorescent CDs@Alg/Cu hydrogel was collected by centrifugation at 300 rpm for 3 min and then washed with deionized water three times.

### Fabrication of silica colloidal crystal beads and PEGDA inverse opal particles

First, template silica colloidal crystal beads (SCCBs) were produced by the self-assembly of $SiO_2$ nanoparticles using a microfluidic device. Then, the obtained SCCBs were dried and immersed into PEGDA solution with 1% wt HMPP added. This step lasted for 4 h to ensure that the pregel liquids sufficiently infiltrated the nanopores of the microparticles. Then, the mixture of microparticles and pregel liquid was exposed to UV light (365 nm, 100 W) for gelation. Last, the remaining hydrogels were removed, and the template SCCBs were etched with hydrofluoric acid (4%, v/v) to successfully generate the PEGDA inverse opal microparticles.

### Generation of the hybrid PEGDA-CDs@Cu/Alg particles

The above CD/alginate aqueous solution was mixed with the PEGDA inverse opal microparticles for 1 h. The liquid blends fully infiltrated into the voids of the inverse opal scaffolds. Then, a 2 mM $CuCl_2$ aqueous solution was added to trigger the gelation of alginate for 2 h to ensure that the microparticles were thoroughly gelated. Finally, the second-filled hybrid PEGDA-CDs@Cu/Alg particles were stripped from the surrounding remaining hydrogels, leaving the PPi-responsive particles behind.

### Effects of PPi on hybrid microparticles

Typically, the as-prepared hybrid PEGDA-CDs@Cu/Alg microparticles were cast into 500 μL of PPi solution with different concentrations (0–3 mM) and mixed well. Then, the system was gently shaken at 150 rpm for 2 h at room temperature. The fluorescent and structural colors of the hybrid microparticles were recorded. To determine the PPi concentration, the microparticles' fluorescence and reflection spectra were acquired using a fiber spectrometer. Two indicators, the emission intensity at 535 nm and the reflection peak value, were used for quantitative analysis of PPi. The same procedures were used for testing the particle responses to other anions.

### Quantitative detection and analysis of ALP

Fifty microliters of PPi (10 mM) was first added to ALP buffer at final concentrations from 0 to 500 mU/mL and mixed well. Then, the blend was incubated at 37 °C for 30 min. After that, the reaction solution was injected into the test tube containing the hybrid PEGDA-CDs@Cu/Alg microparticles for another 2 h at room temperature under gentle shaking at 150 rpm. Finally, the fluorescence and reflection peak positions of the microparticles after the reaction were recorded.

### Characterization

The microstructures of diverse microparticles were characterized by scanning electron microscopy (SEM; Hitachi S3000 N). An optical microscope (Olympus BX51) equipped with a fiber optic spectrometer (Ocean Optics, QE65000) acquired the photographs and reflection spectra. Using a fluorescence microscope (Olympus, CKX41) equipped with a fiber optic spectrometer (Ocean Optics, USB 2000+), we detected the fluorescence intensity of the hydrogel and microparticles.

## Results and discussion

In a typical experiment, alginate gel was first prepared using $Cu^{2+}$ as the crosslinking agent, and its visual response to PPi was verified. Alginate can chelate with $Cu^{2+}$ to form a hydrogel, as shown in Fig. S1. In addition, $Cu^{2+}$ can combine with PPi to generate an ultrastable complex, which triggers a phase change in the copper alginate hydrogel. To characterize this process, CDs were incorporated into the Cu/Alg gel as a fluorescent probe. After excitation by blue light, CDs emit green fluorescence with a maximum emission wavelength at 535 nm. After PPi entered the hydrogel matrix, the gel exhibited a certain degree of disintegration according to the PPi concentration, as shown in Fig. S1. Since CDs leaked from the hydrogel into the destroyed alginate solution, the solutions also showed green fluorescence. We further confirmed the selective response of the hydrogel to PPi by examining the response to eight other anions, including Pis ($H_2PO_4^-$ and $HPO_4^{2-}$), $CO_3^{2-}$, $Cl^-$, $SO_4^{2-}$, $NO_3^-$, $I^-$, and $S^{2-}$, as shown in Fig. S2. No hydrogel disintegration or fluorescence signal was observed in these systems, even when the concentrations of these anions far exceeded that of PPi. This specific response was attributed to the strong competitive coordination effect of PPi on $Cu^{2+}$ compared to other anions.

Then, we fabricated inverse hybrid opal hydrogel microparticles as molecular detection carriers. The particles comprised PEGDA hydrogels via the template etching method from SCCBs (Fig. 1a). The original microparticles were generated through confined assembly from monodisperse silica nanoparticles in microfluidic emulsions. They possessed a finely fraught periodic structure with nanovoids penetrating through the matrix, which facilitated PEGDA liquid infiltration into the voids based on the capillary force. We fabricated the inverse opal particles after polymerizing the PEGDA hydrogel and removing the SCCB template. The PEGDA materials featured high consistency, thereby maintaining the

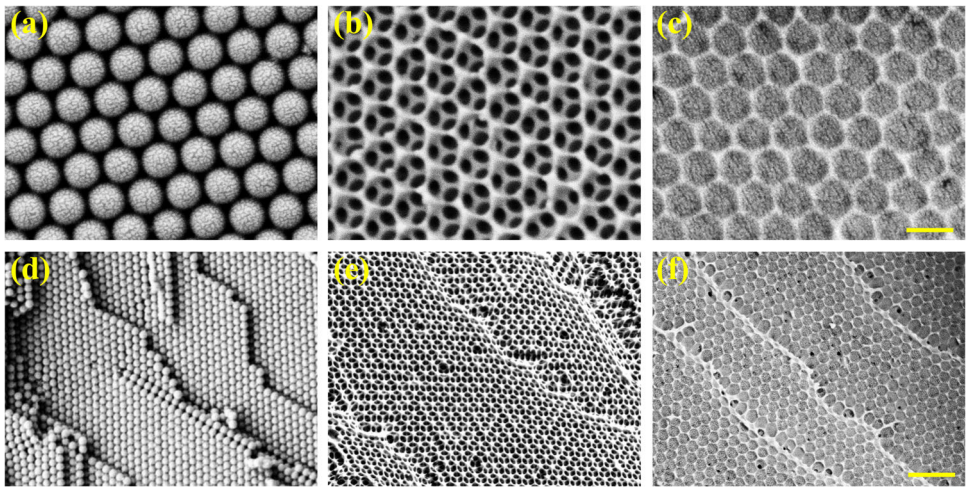


**Fig. 2 Scanning electron microscopy (SEM) characterization of the microstructures of microparticles in the fabrication process. a**, **d** SCCB templates, **b**, **e** PEGDA inverse opal particles, and **c**, **f** hybrid PEGDA-CDs@Cu/Alg particles. In each column, the upper panel depicts the surface of the particle, and the lower panel shows the interior of the particle. The scale bars are 350 nm in **a**–**c** and 1 μm in **d**–**f**.

inverse opal scaffold integrality throughout the following experiments. Afterward, the inverse opal microparticles were dried and immersed in the CDs@Cu/Alg pregel, and then the hybrid structural microparticles were obtained through crosslinking. The SEM images in Fig. 2 showcase the microstructures of the SCCBs, PEGDA inverse opal microparticles, and hybrid PEGDA-CDs@Cu/Alg microparticles. The hexagonal packing structure of $SiO_2$ nanoparticles on the surface of the SCCBs (Fig. 2a) and the nanovoids of the inverse opal microparticles are clearly presented (Fig. 2b). After the voids of the inverse opal microparticles were filled with the CDs@Cu/Alg gel, the hybrid composition of the resultant particles was well characterized, featuring an inverse opal scaffold and a hydrogel filler, as displayed in Fig. 2c.

Due to the ordered structures of the microparticles, the SCCB templates, PEGDA-infiltrated SCCBs, PEGDA inverse opals, and hybrid PEGDA-CDs@Cu/Alg particles were all endowed with certain photonic band gaps (PBGs). Light with specific wavelengths positioned inside the gap would be reflected. As a result, these particles exhibited dazzling structural colors possessing different characteristic reflection peaks. The values of most reflection peak positions $\lambda$ could be calculated according to Bragg's equation[42]:

$$\lambda = 1.633 d n_{average} \quad (1)$$

in which $d$ represents the center-to-center interval between two adjacent building blocks and naverage is the mean refractive index of the system. Thus, SCCBs composed of various nanoparticles possessed distinct structural colors. For example, when $d = 190$, 215, and 260 nm, the color of the SCCBs shifted from blue, green, to red, with $\lambda$ changing from 441 nm, 521 nm, to 611 nm, as shown in Fig. 3a–d. In addition, for a fixed nanoparticle size, the reflection spectrum redshifted from SCCBs, PEGDA-infiltrated SCCBs, and PEGDA inverse opals to hybrid PEGDA-CDs@Cu/Alg particles (Fig. 3e–g) due to the difference in $n_{\mathrm{average}}$. It was noted that the photonic crystal structure of the hybrid hydrogel particles remained intact due to the mechanical strength of the PEGDA matrix. In addition, the green fluorescence of the CDs in the hybrid microparticles could be observed regardless of their reflection peak positions, as shown in Fig. 4. Therefore, the hybrid photonic particles could be used as detection microcarriers providing dual optical indicators (i.e., a fluorescence readout and a structural color readout).

We speculate that the hybrid PEGDA-CDs@Cu/Alg particles would reverse the PPi responsive property, which would cause disintegration of the hydrogel and eventually changes in the dual indicators, fluorescence intensity and reflection peak positions of these microparticles, as depicted in Fig. 4a. To test this hypothesis, a group of particles with $\lambda$ values of 570, 600, and 650 nm were prepared and immersed in 8 mM PPi solution. It was observed that without PPi, the microparticles maintained an intact gel network with full particle fluorescence intensity and no fluorescence signal in the external liquids. Nevertheless, after adding PPi, the outer hydrogel part of the hybrid particles gradually dissociated, resulting in a decrease in the fluorescence intensity due to CD leakage from the particles into the solution, as shown in Figs. 4b–d and S3. In addition, a blueshift of the reflection spectra for the three types of particles was observed. This suggested

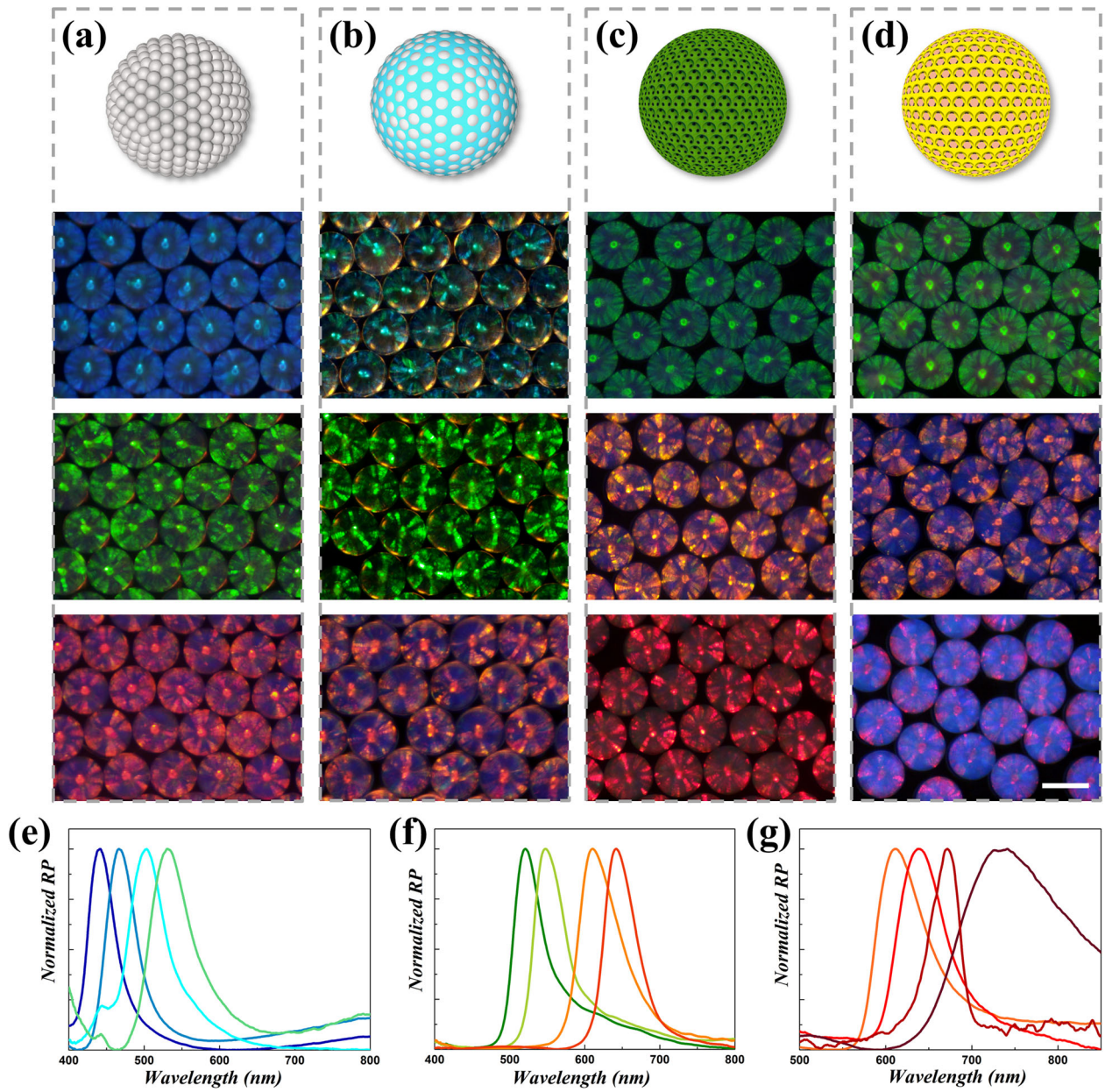


**Fig. 3 Changes in the microparticle structural color and characteristic reflection peaks. a**–**d** Scheme and optical microscopic images of the **a** SCCBs, **b** PEGDA-infiltrated SCCBs, **c** PEGDA inverse opals, and **d** hybrid PEGDA-CDs@Cu/Alg particles. In each column, the images from top to bottom represent particles derived from SCCBs composed of 190, 215, and 260 nm nanoparticles, respectively. **e**–**g** Reflective spectra of the three groups of particles derived from SCCBs composed of **e** 190, **f** 215, and **g** 260 nm nanoparticles. In each image, the lines from left to right represent the spectra of the SCCBs, PEGDA-infiltrated SCCBs, PEGDA inverse opals, and hybrid PEGDA-CDs@Cu/Alg particles, respectively. All scale bars are 200 μm.

that the PPi-triggered phase transformation of the CDs@Cu/Alg hydrogel led to a change in the mean index of refraction of the hybrid microparticles as a function of Eq. (1). In addition, 2 h after the addition of PPi, the outer hydrogel of the microparticles was almost dissociated and had reached the platform. The reaction time employing common methods is provided in Table S1.

A quantitative study of changes in these dual optical indicators as a function of the PPi concentration was further conducted. Figure 5a shows that when 4 mM PPi was added, the edges of the particles became blurred, which was accompanied by a sharp decrease in fluorescence intensity as measured by the average of all microparticles. This suggested that the surface of the particles

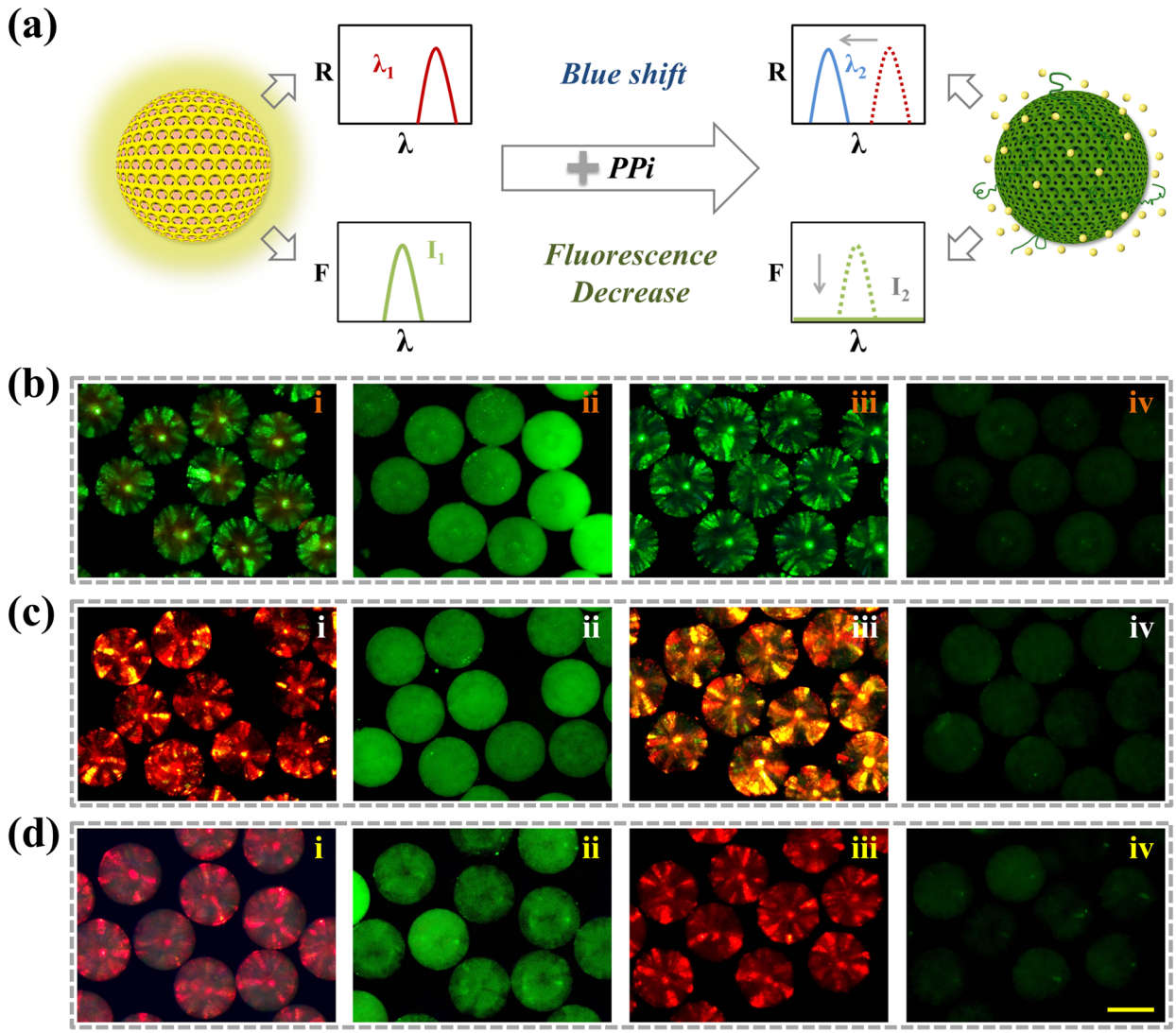


**Fig. 4 Dual-signal response of hybrid PEGDA-CDs@Cu/Alg particles to PPi. a** Scheme of the dual response of the photonic particles to PPi: the blueshift phenomenon in the reflection spectra and the decrease in fluorescence intensity are due to the disintegration of the CDs@Cu/Alg hydrogel. **b**–**d** Optical microscopy images (i) and corresponding fluorescence images (ii) of three kinds of hybrid PEGDA-CDs@Cu/Alg particles before the addition of PPi and optical microscopy images (iii) and corresponding fluorescence images (iv) of the particles after treatment with 8 mM PPi. The λ values of the primary hybrid hydrogel microparticles were (bi) 570, (ci) 600, and (di) 650 nm. After reacting with PPi, there was corresponding shifts to (biii) 540, (ciii) 576, and (diii) 622 nm. All scale bars are 200 μm.

disintegrated upon contacting PPi. We plotted the average fluorescent intensity of the hybrid PEGDA-CDs@Cu/Alg microparticles according to the PPi concentration and then obtained a detection limit of 37.24 μM and a linearity range from 0.1 to 4 mM with a correlation coefficient of 0.9974 (Fig. 5b and Fig. S4). The simultaneous blueshift of the reflection spectra of the particles corresponding to an increase in the PPi concentration was measured, as shown in Fig. 5c. A distinguishable color change of the particles was observed, with the reflection peak value decreasing gradually and saturating when the concentration of PPi reached 10 mM.

Based on the PPi-response behavior of the prepared hybrid photonic particles, we developed a dual-signal ALP sensing platform. ALP serves as a representative hydrolase that can transform one PPi to two Pis. This could suppress the combination of PPi and $Cu^{2+}$ and thus reduce the destructive effect of the CDs@Cu/Alg hydrogel. As confirmed in Fig. S5, the particles treated with a mixture of PPi and ALP showed a smaller decrease in fluorescence than those treated with PPi alone. As a control, the particles treated with only ALP maintained an intact microsphere structure, and the original fluorescence was maintained even when the concentration of ALP was

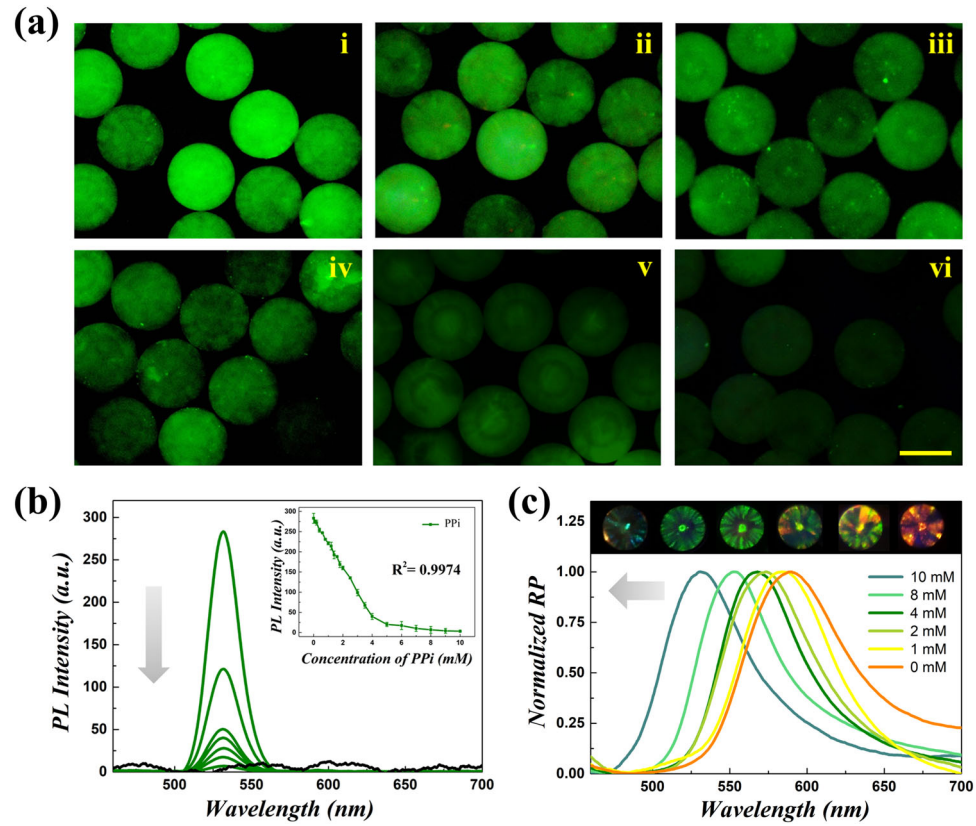


**Fig. 5 Fluorescence intensities and reflection curves of the hybrid PEGDA-CDs@Cu/Alg microparticles with different PPi concentrations.** **a** Fluorescence images of the hybrid hydrogel microparticles in response to different concentrations of PPi. From i to vi: 0, 1, 2, 4, 6, and 8 mM, respectively. **b** Fluorescence spectra of the microparticles after treatment with different PPi concentrations (0, 1, 2, 4, 6, 8, 9, and 10 mM). The inset shows the plot of the fluorescence intensity at 535 nm according to the PPi concentration. **c** Reflection spectra of the microparticles with an initial reflection peak value at 589 nm after treatment with PPi concentrations of 0, 1, 2, 4, 8, and 10 mM. The scale bar in **a** is 200 μm.

500 mU/mL. Thus, PPi was the direct stimulus signal that caused the phase and fluorescence change in the CDs@Cu/Alg hydrogel, and ALP was the indirect stimulus signal that degraded PPi to suppress these changes. These results indicated that the prepared hybrid structural microparticles with CDs@Cu/Alg hydrogel could serve as desirable ALP sensors.

To evaluate the detection sensitivity of ALP, we incubated the particles in a mixture of PPi with ALP and measured the fluorescence intensity as a function of ALP concentration. As shown in Fig. 6a, the fluorescence of the particles increased with increasing ALP concentration. With the presence of 10 mM PPi in the detection solution, we drew a calibration curve and identified a linear relationship between the fluorescence intensity and ALP concentration in the range from 1 to 150 mU/mL (Fig. 6b). The detection limit of this system was 0.87 mU/mL after calculation, which was comparable to that previously reported (Table S1)[43]. In addition, a higher concentration of ALP led to a redshift of the reflection spectra (Fig. 6c). The detection limit measured by this method was 1.21 mU/mL (Fig. 6d), which is comparable to that of fluorescence detection. It is worth mentioning that increasing the number of microparticles is similar to enlarging the total amount of CDs@Cu/Alg gel, which has the same effect on fluorescence and structural color signals as decreasing the concentration of PPi or increasing the concentration of ALP in the system. However, this operation can improve the uniformity of the reaction, thus accelerating the arrival of the plateau. Such a dual-signal sensing platform provided a wider detection range and a more reliable detection result.

## Conclusion

In conclusion, we presented hybrid alginate photonic microparticles for ALP detection. The detection mechanism was based on an intermediary chemical, PPi, that could trigger the phase transition of the alginate hydrogel due to competitive combination with the hydrogel crosslinker, $Cu^{2+}$. ALP could react with PPi and thus suppress the phase transition. This responsive

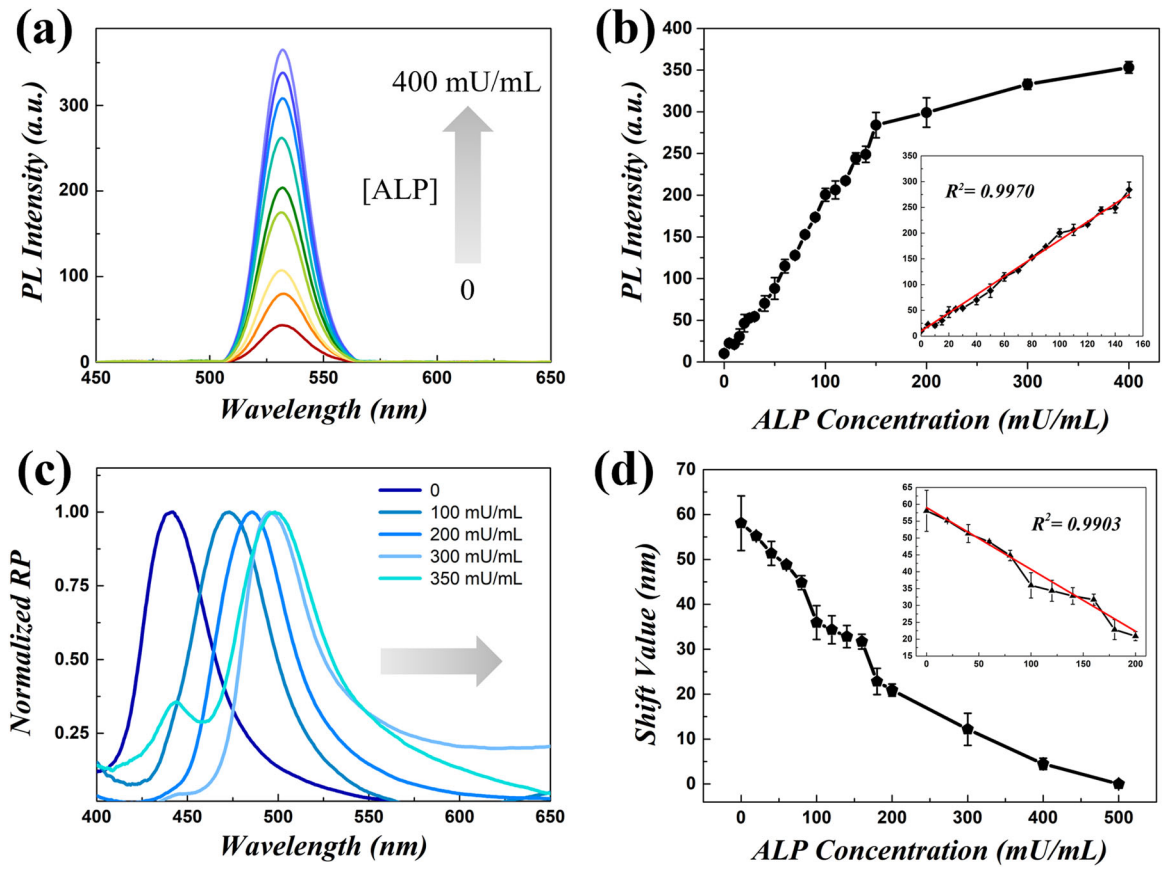


**Fig. 6 Dual signal detection of ALP. a** Fluorescence spectra of the hybrid microparticles after treatment with a mixture of 10 mM PPi and different ALP concentrations (0–400 mU/mL). **b** A linear curve of fluorescent intensity at 535 nm versus ALP concentration. **c** Reflection spectra of the particles with an initial reflection peak value at 441 nm (without ALP) immersed in a mixture of 10 mM PPi and different concentrations of ALP (0, 100, 200, 300, and 350 mU/mL). **d** The measured reflection peak shift value as a function of ALP concentration.

behavior was converted to dual optical signals for the detection of ALP. CDs were integrated into the particles to give a fluorescence readout. Additionally, the particles were generated with a unique photonic crystal structure and provided structural color that served as an additional readout. The detection limit of these two strategies were 0.87 mU/mL and 1.21 mU/mL, respectively, with high selectivity in comparison to other proteins and biological specials. Compared with the previous method applying bulk hydrogel sensors as visual indicators for ALP detection, the hybrid photonic microparticles possess flexible motor behaviors that provide higher reaction uniformity and reduce duration. Additionally, such a dual-indicator platform could enhance the reliability of the detection results. However, the relatively high cost and complicated manufacturing process are drawbacks compared to the inexpensive bulk hydrogel. These features, together with other merits, including biocompatibility, make photonic hybrid hydrogel particles a promising platform for the detection of ALP and other macromolecules.

**Acknowledgements**
This work was supported by the National Key Research and Development Program of China (2020YFA0908200), the National Natural Science Foundation of China (22002018, 52073060, and 61927805), and the Shenzhen Fundamental Research Program (JCYJ20190813152616459 and JCYJ20210324133214038).

**Author details**
[1]Department of Rheumatology and Immunology, Nanjing Drum Tower Hospital, School of Biological Science and Medical Engineering, Southeast University, 210096 Nanjing, China. [2]School of Food Science and Pharmaceutical Engineering, Nanjing Normal University, 210046 Nanjing, China. [3]Shanghai Xuhui Central Hospital, Zhongshan-Xuhui Hospital, and the Shanghai Key Laboratory of Medical Epigenetics, the International Co-laboratory of Medical Epigenetics and Metabolism (Ministry of Science and Technology), Institutes of Biomedical Sciences, Fudan University, 200032 Shanghai, China

**Author contributions**
Y.Z. and L.S. conceived the idea and designed the experiment. Y.W. and D.Z. conducted the experiments and data analysis. Y.W. wrote the manuscript. H.Z., L.S., and Y.Z. assisted with the writing of the manuscript.

**Conflict of interest**
The authors declare no competing interests.

**Supplementary information** The online version contains supplementary material available at https://doi.org/10.1038/s41427-022-00401-8.

Received: 16 March 2022 Revised: 9 May 2022 Accepted: 18 May 2022.
Published online: 24 June 2022

## References

1. He, H. J. et al. Enzymatic noncovalent synthesis. *Chem. Rev.* **18**, 9994–10078 (2020).
2. Krzyzosiak, A. et al. Target-based discovery of an inhibitor of the regulatory phosphatase PPP1R15B. *Cell* **174**, 1216–1228 (2018).
3. Ou, P. et al. Gasotransmitter regulation of phosphatase activity in live cells studied by three-channel imaging correlation. *Angew. Chem. Int. Ed.* **58**, 2261–2265 (2019).
4. Tonks, N. K. Protein tyrosine phosphatases: from genes, to function, to disease. *Nat. Rev. Mol. Cell. Biol.* **7**, 833–846 (2006).
5. Han, Y., Chen, J., Li, Z., Chen, H. & Qiu, H. Recent progress and prospects of alkaline phosphatase biosensor based on fluorescence strategy. *Biosens. Bioelectron.* **148**, 111811 (2020).
6. Shi, D. et al. Naked-eye sensitive detection of alkaline phosphatase (ALP) and pyrophosphate (PPi) based on a horseradish peroxidase catalytic colorimetric system with Cu(ii). *Analyst* **141**, 5549–5554 (2016).
7. Hai, Z., Li, J., Wu, J., Xu, J. & Liang, G. Alkaline phosphatase-triggered simultaneous hydrogelation and chemiluminescence. *J. Am. Chem. Soc.* **139**, 1041–1044 (2017).
8. Díaz, A. N., Sánchez, F. G., Ramos, M. & Torijas, M. Horseradish peroxidase sol gel immobilized for chemiluminescence measurements of alkaline-phosphatase activity. *Sens. Actuat. B-Chem* **82**, 176–179 (2002).
9. Goggins, S., Naz, C., Marsh, B. J. & Frost, C. G. Ratiometric electrochemical detection of alkaline phosphatase. *Chem. Commun.* **51**, 561–564 (2015).
10. Ino, K. et al. Novel electrochemical methodology for activity estimation of alkaline phosphatase based on solubility difference. *Anal. Chem.* **84**, 7593–7598 (2012).
11. Ruan, C., Wang, W. & Gu, B. Detection of alkaline phosphatase using surface-enhanced Raman Spectroscopy. *Anal. Chem.* **78**, 3379–3384 (2006).
12. Wang, X. Y., Jiang, X. Q. & Wei, H. Phosphate-responsive 2D-metal–organic-framework-nanozymes for colorimetric detection of alkaline phosphatase. *J. Mater. Chem. B* **8**, 6905–6911 (2020).
13. Zhao, C. Q. et al. Plasmonic enhanced gold nanoclusters-based photoelectrochemical biosensor for sensitive alkaline phosphatase activity analysis. *Anal. Chem.* **92**, 6886–6892 (2020).
14. Xiang, M. H. et al. A fluorescent graphitic carbon nitride nanosheet biosensor for highly sensitive, label-free detection of alkaline phosphatase. *Nanoscale* **8**, 4727–4732 (2016).
15. Niu, X., Ye, K., Wang, L., Lin, Y. & Du, D. A review on emerging principles and strategies for colorimetric and fluorescent detection of alkaline phosphatase activity. *Anal. Chim. Acta* **1086**, 29–45 (2019).
16. Wang, K. et al. Fluorescent probes for the detection of alkaline phosphatase in biological systems: recent advances and future prospects. *Trac-Trend Anal. Chem.* **136**, 116189 (2021).
17. Chen, C., Zhao, J., Lu, Y., Sun, J. & Yang, X. Fluorescence immunoassay based on the phosphate-triggered fluorescence turn-on detection of alkaline phosphatase. *Anal. Chem.* **90**, 3505–3511 (2018).
18. Freeman, R., Finder, T., Gill, R. & Willner, I. Probing Protein Kinase (CK2) and alkaline phosphatase with Cdse/Zns Quantum dots. *Nano Lett.* **10**, 2192–2196 (2010).
19. Yang, W., Luo, J., Qi, M. & Yang, M. Detection of alkaline phosphatase activity and inhibition with fluorescent hydroxyapatite nanoparticles. *Anal. Methods* **11**, 2272–2276 (2019).
20. Yang, J. et al. Guanine-rich DNA-based peroxidase mimetics for colorimetric assays of alkaline phosphatase. *Biosens. Bioelectron.* **77**, 549–556 (2016).
21. Jiao, H. et al. Nucleic acid-regulated perylene probe-induced gold nanoparticle aggregation: a new strategy for colorimetric sensing of alkaline phosphatase activity and inhibitor screening. *ACS Appl. Mater. Interfaces* **6**, 1979–1985 (2014).
22. Liu, Q. et al. Ultrasensitive detection alkaline phosphatase activity using 3-aminophenylboronic acid functionalized gold nanoclusters. *Actuat. B-Chem.* **281**, 175–181 (2019).
23. Zhu, Z. et al. Microfluidics-assisted assembly of injectable photonic hydrogels toward reflective cooling. *Small* **16**, 1903939 (2020).
24. Shao, C. M. et al. Photo-controllable inverse opal graphene hydrogel scaffolds with biomimetic enrichment capability for cell culture. *Research* **2019**, 9783793 (2019).
25. Li, J. & Mooney, D. J. Designing hydrogels for controlled drug delivery. *Nat. Rev. Mater.* **1**, 16071 (2016).
26. Liu, Z., Wang, W., Xie, R., Ju, X. J. & Chu, L. Y. Stimuli-responsive smart gating membranes. *Chem. Soc. Rev.* **45**, 460–475 (2016).
27. Mao, Y. et al. A portable visual detection method based on a target-responsive DNA hydrogel and color change of gold nanorods. *Chem. Commun.* **53**, 6375–6378 (2017).
28. Mao, X. et al. Self-healing and Injectable Hydrogel for Matching Skin Flap Regeneration. *Adv. Sci.* **6**, 1801555 (2019).
29. Yan, L. et al. Target-responsive "sweet" hydrogel with glucometer readout for portable and quantitative detection of non-glucose targets. *J. Am. Chem. Soc.* **135**, 3748–3751 (2013).
30. Hou, J., Li, M. Z. & Song, Y. L. Patterned colloidal photonic. *Cryst. Angew. Chem. Int. Ed.* **57**, 2544–2553 (2018).
31. Cai, L. J. et al. Stomatocyte structural color-barcode micromotors for multiplex assays. *Natl Sci. Rev.* **7**, 644–651 (2020).
32. Chen, C. W. et al. Multifunctional chitosan inverse opal particles for wound healing. *ACS Nano* **12**, 10493–10500 (2016).
33. Zhang, Y., Zhu, C. & Xia, Y. Inverse opal scaffolds and their biomedical applications. *Adv. Mater.* **29**, 1701115 (2017).
34. Fu, Q. Q., Zhu, H. M. & Ge, J. P. Electrically tunable liquid photonic crystals with large dielectric contrast and highly saturated structural colors. *Adv. Funct. Mater.* **28**, 1804628 (2018).
35. Hou, J., Li, M. Z. & Song, Y. L. Recent advances in colloidal photonic crystal sensors: materials, structures and analysis methods. *Nano Today* **22**, 132–144 (2018).
36. Zhang, H. et al. Immunotherapeutic silk inverse opal particles for post-surgical tumor treatment. *Sci. Bull.* **65**, 380–388 (2020).
37. Zhao, Y. et al. PH- and temperature-sensitive hydrogel nanoparticles with dual photoluminescence for bioprobes. *ACS Nano* **10**, 5856–5863 (2016).
38. Liu, Y. X. et al. Bioinspired structural color particles with multi-layer graphene oxide encapsulated nanoparticle components. *Bioact. Mater.* **5**, 917–923 (2020).
39. Xu, C., Ren, J., Feng, L. & Qu, X. $H_2O_2$ triggered sol–gel transition used for visual detection of glucose. *Chem. Commun.* **48**, 3739–3741 (2012).
40. Li, M. Z., Lai, X., Li, C. & Song, Y. L. Recent advantages of colloidal photonic crystals and their applications for luminescence enhancement. *Mater. Today Nano* **6**, 100039 (2019).
41. Huang, Y. et al. Target-responsive DNA enzyme cross-linked hydrogel for visual quantitative detection of lead. *Anal. Chem.* **86**, 11434–11439 (2014).
42. Zhang, H. et al. Responsive drug-delivery microcarriers based on the silk fibroin inverse opal scaffolds for controllable drug release. *Appl. Mater. Today* **19**, 100540 (2020).
43. Li, Y., Huang, Z. Z., Weng, Y. H. & Tan, H. L. Pyrophosphate ion-responsive alginate hydrogel as an effective fluorescent sensing platform for alkaline phosphatase detection. *Chem. Commun.* **55**, 11450–11453 (2019).